Vanadium Oxides

DOI: 10.1002/anie.200905227

Direct Confined-Space Combustion Forming Monoclinic Vanadium Dioxides**

*Changzheng Wu, Jun Dai, Xiaodong Zhang, Jinlong Yang, Fei Qi, Chen Gao, and Yi Xie**

Monoclinic vanadium dioxides VO_2(M) are prototype materials for interpreting correlation effects in solids.[1] Moreover, VO_2(M) undergoes a fully reversible metal–insulator phase transition between monoclinic VO_2(M) and rutile vanadium dioxide VO_2(R) (Supporting Information S1) with the benefits of huge temperature-induced changes in resistivity and selective optical switching, and has thus attracted great interest in the industrial and scientific communities for construction of intelligent devices such as temperature sensors and energy-efficient smart windows.[2,3] For more than 50 years after Morin's discovery,[4] solid-state reactions were regarded as the exclusive synthetic route to VO_2(M).[5,6] Obtaining VO_2(M) as the product of a solid-state reaction usually requires the rigid synergic effects of high-temperature post-treatment, inert-gas atmosphere with precisely controlled flow, and long synthesis time, and this has made VO_2(M) one of the most expensive metal oxides up to now (Supporting Information S2).

Since the conventional synthesis temperature for functional oxides is usually higher than the phase transition temperature of about 68 °C, it is thought VO_2(M) can be formed solely by phase transition from the high-temperature VO_2(R) phase, and that controlling the formation of the VO_2(R) phase is the exclusive way of forming VO_2(M). VO_2(R) is well known as the thermodynamically most stable phase among the tens of kinds of vanadium dioxides.[7,8] It consists of VO_6 octahedra that share two opposite parallel edges to form octahedral chains, which stack by sharing corners to form VO_2(R).[9] The as-formed highly symmetric structure of VO_2(R), in which the vanadium atoms are at the centers of regular oxygen octahedra, is regarded to be a more stable structure. Other VO_2 polymorphs besides VO_2(R) usually have a shear structure[10] in which deformed oxygen octahedra with vanadium atoms no longer at their center lead to metastable structures. Among these metastable structures, VO_2(B) is well known as the most common phase from solution reactions.[11,12] In this regard, we calculated the formation energy for VO_2(R) and VO_2(B) on the basis of density functional calculations (Supporting Information S3). Per [VO_2] unit, VO_2(R) has a lower formation energy (5.611 eV) than VO_2(B). These calculation results further provide theoretical support for VO_2(R) as the thermodynamically stable phase.

Herein we report a new method to obtain VO_2(M), by direct combustion of an ethanolic solution of $VO(acac)_2$ (acac = acetylacetonate) in a confined space (Figure 1). In our approach, the alcohol combustion in a confined space provides both sufficient thermal energy and a reducing/inert atmosphere, to overcome the reaction barrier and keep vanadium in the +4 valence state, respectively, and it leads to exclusive formation of thermodynamically stable VO_2(R). Since the phase transition between VO_2(M) and VO_2(R) is fully reversible, monoclinic VO_2(M) is formed from VO_2(R) when the product cools to room temperature. The whole process to form VO_2(M) only involves an appropriately sized beaker and an ethanolic solution containing $VO(acac)_2$, offers high convenience, short reaction time, "green" chemistry, and no need for any complex manipulations or equipment.

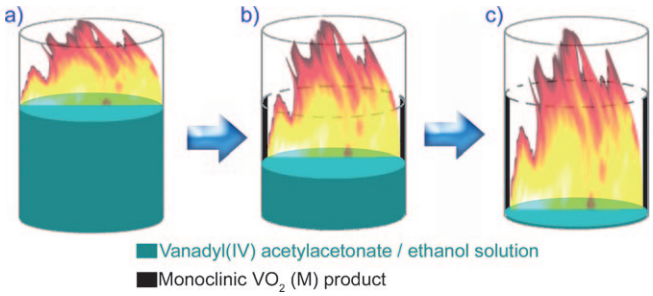

Figure 1. Direct confined-space combustion to give monoclinic VO_2(M).

The XRD pattern of the synthetic product (Figure 2a) matches well with that of standard JCPDS card No. 43-1051 corresponding to monoclinic VO_2(M) with space group $P2_1c$. The XRD pattern calculated from the VO_2(M) crystal cell (Figure 2a) is identical to the experimental pattern, and this provides direct evidence for the monoclinic phase of VO_2. The HRTEM image and selected area electron diffraction (SAED) pattern (Figure 2c and d) of the particle edge provided information on the phase of the product. The angle of 90° between the (020) and (100) planes is fairly consistent with that calculated from the crystallographic parameters of

[*] Dr. C. Z. Wu, Dr. J. Dai, Dr. X. D. Zhang, Prof. J. L. Yang, Prof. Y. Xie
Hefei National Laboratory for Physical Sciences at the Microscale
University of Science & Technology of China
Hefei, Anhui 230026 (P.R. China)
Fax: (+86) 551-360-3987
E-mail: yxie@ustc.edu.cn
Prof. F. Qi, Prof. C. Gao
National Synchrotron Radiation Laboratory
University of Science & Technology of China
Hefei, Anhui 230029 (P.R. China)

[**] This work was financially supported by the National Basic Research Program of China (No. 2009CB939901), National Natural Science Foundation of China (No. 20801051, 90922016), and innovation project of Chinese Academy of Science (KJCX2-YW-H2O).

Supporting information for this article is available on the WWW under http://dx.doi.org/10.1002/anie.200905227.

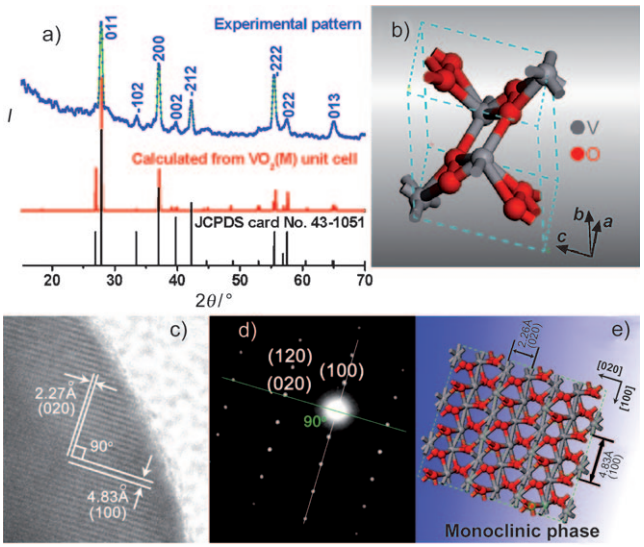

Figure 2. a) Experimental XRD pattern, calculated XRD pattern achieved from the unit cell of VO_2(M), and standard pattern in JCPDS card No. 43-1051. b) Unit cell of VO_2(M) product. HRTEM image (c) and SAED pattern (d) taken on a typical VO_2(M) particle. e) Atomic model with the same projected direction as in the HRTEM image.

monoclinic VO_2 and an atomic model (Figure 2e) with the same projected direction as in the HRTEM image, and this is further solid evidence for monoclinic VO_2.

The quality and composition of the VO_2(M) sample were further characterized by X-ray photoelectron spectroscopy (XPS) and Raman spectroscopy. The XPS spectra show that the as-obtained sample consists of vanadium and oxygen, with the carbon peak at 284.6 eV as reference. Also, the V2p core-level spectrum (Supporting Information Figure S4-1b) shows that the observed value of the binding energy (516.4 eV) for $V_{2p3/2}$ is in good agreement with the literature values of bulk-phase V^{4+}.[13,14] In addition, the binding energy difference (Δ) between the O1s and $V2p_{3/2}$ level was also used to determine the oxidation state of the vanadium oxide.[15] The Δ value of the present VO_2(M) sample of 13.6 eV approaches that reported in the literature for V^{4+}.[15,16] The XPS spectra clearly reveal that in the as-obtained sample vanadium is in the +4 valence state, without any presence of the +5 valence state. Moreover, in the Raman spectrum (Supporting Information, Figure S4-2), the absence of the typical G band and D bands, which usually correspond to the E2g modes of graphite and disordered graphite or glassy carbon, respectively, clearly verifies the absence of carbon-based species in our sample. Thus, both XP and Raman spectra confirm the high quality of the as-obtained VO_2(M) sample.

In the synthetic reaction, monoclinic VO_2 is obtained by ethanol-flame-induced pyrolysis of an initially formed VO(acac)$_2$ film. During solvent consumption by combustion, surface accumulation of solute VO(acac)$_2$ results in a thin blue film of VO(acac)$_2$ on the glass inner wall by a process similar to colloidal pattern formation by solvent drying.[17,18] With increasing ethanol consumption by combustion, the air/solution interface gradually drops, the ethanol flame can directly ignite the VO(acac)$_2$ film, and pyrolysis of VO(acac)$_2$ leads to formation of monoclinic VO_2 on the beaker-wall substrate. In fact, the vanadium valence state and the flammable ligands play a vital role in the formation of VO_2(M) product (Supporting Information S5).

Moreover, ethanol combustion in a confined space provides both sufficient thermal energy and the reducing/inert reaction atmosphere to facilitate the formation of VO_2(M). In the formation mechanism of VO_2(M), ethanol combustion provides sufficient thermal energy to overcome the energy barrier for formation of the thermodynamically stable monoclinic phase of VO_2. Sufficiently high temperature is usually necessary for formation of the thermodynamically stable phase. In our case, the high-temperature reaction conditions come from ethanol combustion. Thermal infrared images were used to directly observe the spatial distribution of temperature during the reaction (Figure 3a). The high-

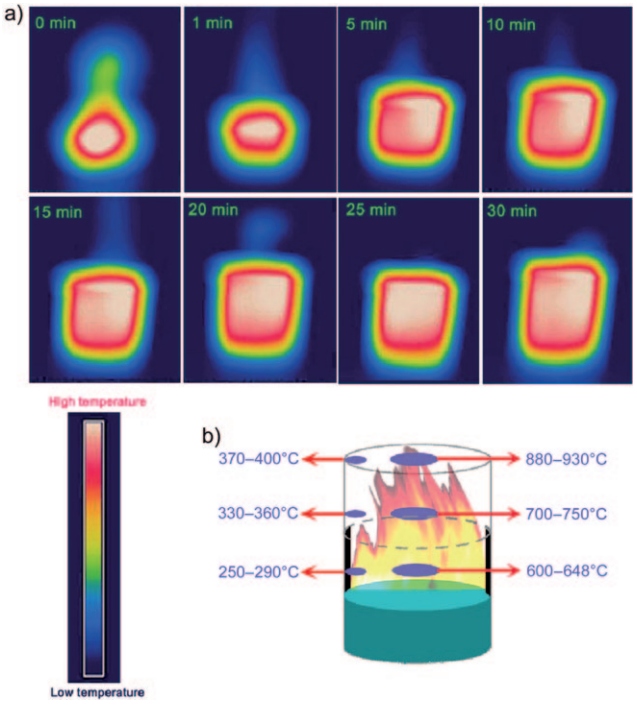

Figure 3. a) Evolution of spatial temperature distribution with reaction time in the confined space of the beaker, captured from the side by a thermal infrared camera. b) Schematic illustration of the temperature distribution for inner wall surface and the center of the beaker, measured by thermocouple detector.

temperature region lies at the center of the glass beaker, and the temperature gradually drops on moving away from the central position in the initial stage of the reaction. The high-temperature region extends further downward as the air/liquid interface falls with proceeding ethanol consumption. At the end of the reaction stage, the high-temperature region even expands into the whole beaker and the red color corresponding to high temperature exhibits the shape of the beaker.

We measured the temperature distribution in the reaction space with a thermocouple detector as shown in Figure 3b. Due to the presence of sufficient oxygen, the temperature at the open end of the beaker is usually higher than that at

deeper points. The central point at the open end of the beaker has a temperature of 880–930 °C, while those of two lower points were 700–750 and 600–648 °C. The temperature on the inner beaker wall is lower than that of the central region due to significant thermal radiation of the glass wall. The inner wall at the open end still has the highest temperature of 370–400 °C, while the lower lying regions of the inner wall have the lower values of 330–360 and 250–290 °C. The temperature data measured by thermocouple are in fair agreement with the temperature gradient in the thermal infrared images (Figure 3a) along the radial and axial directions of the beaker, and this is further confirmation of the higher temperature in the confined space of the beaker. In other words, ethanol combustion in confined space provides sufficient thermal energy to ensure formation of thermodynamically stable monoclinic phase of VO_2.

Moreover, confined-space ethanol combustion also provides a reducing/inert atmosphere that prevents oxidation of monoclinic VO_2 to V^{5+} oxides. To identify the intermediates and products of the ethanol flame, we performed experiments on premixed stoichiometric ethanol/oxygen flames and pyrolysis of ethanol with tunable synchrotron vacuum ultraviolet (VUV) photoionization mass spectrometry (Figure 4 and Table S6 in the Supporting Information). The mass spectra clearly show that the dominant intermediate species in the ethanol flame, such as alcohol, aldehyde, H_2 and CO, are reductive and inert with respect to the valence state of vanadium (Supporting Information S6). Vanadium(IV) is usually sensitive to oxidation to V^V in air at high temperature (usually > 300 °C),[19] but the reducing/inert atmosphere in the confined space of the beaker prevents oxidation of the V^{IV} oxide product to the V^V valence state. Kohse-Höinghaus and co-workers used metal acetylacetonate/ethanol solutions to grow high-quality transition metal thin films by ethanol-assisted chemical vapor deposition, in which the similar reducing effects were also present during the reaction.[20,21] In summary, the above-mentioned two synergic effects of ethanol combustion favor formation of thermally stable VO_2(R), which transforms into VO_2(M) on cooling to room temperature.

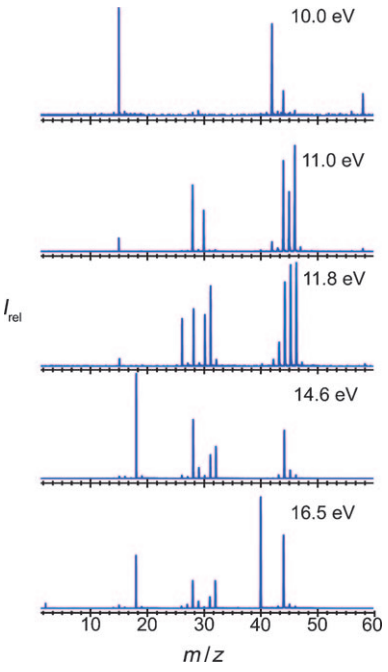

Figure 4. Synchrotron-radiation photoionization mass spectra measured on samples from the luminous zone of a premixed ethanol/oxygen flame. VUV photon energies [eV] are indicated in the figures.

The reversible phase transition of VO_2(M) is clearly revealed by the temperature-dependent resistivity curve, zero-field cooled (ZFC) magnetization curve, and differential scanning calorimetry (DSC) curves. The variation in electrical resistance with temperature clearly shows an abrupt drop around 67 °C (Figure 5a) and a heating–cooling hysteresis of about 5 °C. Also, the ZFC magnetization curve (Figure 5b) shows sharp increase in magnetic susceptibility around 67.8 °C, which clearly indicates the structural phase change. The simultaneous decreases in magnetic susceptibility and electrical conductivity suggest formation of charge-density waves or a spin Peierls transition in VO_2(M).[22,23]

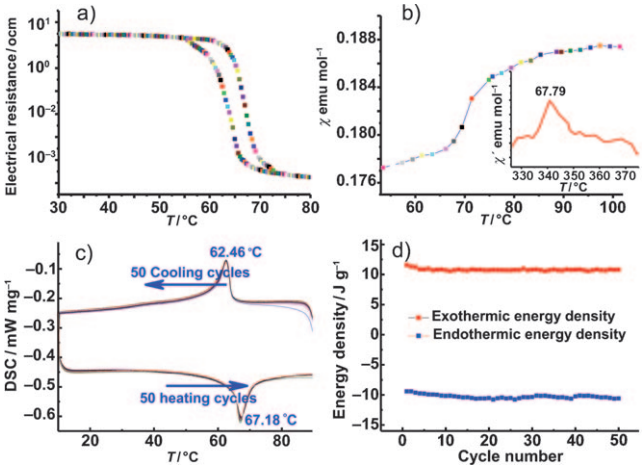

Figure 5. a) Temperature dependence of the resistivity of VO_2(M). b) ZFC magnetization as a function of temperature. Inset: differential curve of the ZFC curves in an applied magnetic field of 200 Oe. c) DSC thermal spectra of as-obtained VO_2(M) from the 1st to the 50th cycle. d) Cycling behavior of exothermic (red) and endothermic (blue) energy density for as-obtained VO_2(M).

The first-order phase transition from rutile to monoclinic VO_2 usually involves a substantial entropy component. During the phase transition, under the driving force of decreasing temperature, a small distortion of infinite V^{4+}–V^{4+} chains in rutile VO_2 occurs to form zigzag V^{4+}–V^{4+} pairs that no longer linearly arrange in monoclinic VO_2(M). In this case, the small distortion of the atomic lattice and the change in conduction electrons are responsible for the entropy change due to discontinuity of the carrier density.[24] Therefore, thermal analysis studies reveal the direct character of the first-order structural transition in VO_2. Figure 5c shows the DSC curves for as-obtained VO_2(M), which shows a narrow heating–cooling hysteresis of about 4.72 °C and excellent cycling behavior for the structural phase transition. Fifty

heating and cooling cycles were all coincident, with no obvious deviation or distortion of the DSC curves. Also, the cycling behavior of exothermic and endothermic energy density (Figure 5d) further confirms the excellent exothermal and endothermal stability of the metal–insulator transition of as-obtained VO_2(M). In other words, the sharp increases in temperature-dependent resistivity and ZFC magnetization clearly mark the structural phase change, while the narrow heating–cooling hysteresis of the DSC curves and the excellent exothermal and endothermal stability suggests that our synthetic monoclinic VO_2 product is of high quality.

In summary, direct combustion of an ethanolic solution of $VO(acac)_2$ in a confined space affords monoclinic VO_2(M) and brings this expensive material into the realm of conventional laboratory synthesis. The whole process is remarkably convenient, with short reaction time, "green" chemistry, and no need for any complex equipment or manipulations. Real-time thermal infrared images and synchrotron-radiation photoionization mass spectra clearly reveal the dual role of ethanol in the reaction system. Moreover, since VO_2(M) is a prototype material for interpreting correlation effects in solids, the present synthesis of high-quality VO_2(M) provides a solid basis to settle the long-running debate[1,2] over the roles played by lattice distortion and electron–electron correlation in the temperature-driven metal–insulator transition, as well as for construction of intelligent devices such as temperature sensors and energy-efficient smart windows.

Experimental Section

VO_2(M): 2 mmol of $VO(acac)_2$ was loaded into a beaker (diameter: 50 mm; height: 70 mm) containing 40 mL of absolute ethanol. The $VO(acac)_2$ solution became transparent after strong stirring. The ethanolic solution was directly ignited and allowed to combust completely, and VO_2(M) was obtained in as a film on the inner wall of the beaker.

Received: September 18, 2009
Published online: November 26, 2009

Keywords: high-temperature chemistry · oxidation · oxides · synthetic methods · vanadium

[1] P. Baum, D. S. Yang, A. H. Zewail, *Science* **2007**, *318*, 788.
[2] M. M. Qazilbash, M. Brehm, B. G. Chae, P. C. Ho, G. O. Andreev, B. J. Kim, S. J. Yun, A. V. Balatsky, M. B. Maple, F. Keilmann, H. T. Kim, D. N. Basov, *Science* **2007**, *318*, 1750.
[3] J. Wei, Z. H. Wang, W. Chen, D. H. Cobden, *Nat. Nanotechnol.* **2009**, *4*, 420.
[4] F. J. Morin, *Phys. Rev. Lett.* **1959**, *3*, 34.
[5] B. S. Guiton, Q. Gu, A. L. Prieto, M. S. Gudiksen, H. K. Park, *J. Am. Chem. Soc.* **2005**, *127*, 498.
[6] L. Whittaker, C. Jaye, Z. G. Fu, D. A. Fischer, S. Banerjee, *J. Am. Chem. Soc.* **2009**, *131*, 8884.
[7] G. Andersson, *Acta Chem. Scand.* **1954**, *8*, 1599.
[8] Z. Gui, R. Fan, X. H. Chen, Y. C. Wu, *J. Solid State Chem.* **2001**, *157*, 250.
[9] C. Leroux, G. Nihoul, G. V. Tendeloo, *Phys. Rev. B* **1998**, *57*, 5111.
[10] H. Katzke, P. Toledano, W. Depmeier, *Phys. Rev. B* **2003**, *68*, 024109.
[11] S. A. Corr, M. Grossman, Y. F. Shi, K. R. Heier, G. D. Stucky, R. Seshadri, *J. Mater. Chem.* **2009**, *19*, 4362.
[12] J. F. Liu, Q. H. Li, T. H. Wang, D. P. Yu, Y. D. Li, *Angew. Chem.* **2004**, *116*, 5158; *Angew. Chem. Int. Ed.* **2004**, *43*, 5048.
[13] G. A. Sawatzky, D. Post, *Phys. Rev. B.* **1979**, *20*, 1546.
[14] C. Z. Wu, Z. P. Hu, W. Wang, M. Zhang, J. L. Yang, Y. Xie, *Chem. Commun.* **2008**, 3891.
[15] J. Mendialdua, R. Casanova, Y. J. Barbaux, *Electron. Spectrosc. Relat. Phenom.* **1995**, *71*, 249.
[16] G. A. Sawatzky, D. Post, *Phys. Rev. B* **1979**, *20*, 1546.
[17] E. Rabani, D. R. Reichman, P. L. Geissler, L. E. Brus, *Nature* **2003**, *426*, 271.
[18] A. K. Bohaty, I. Zharov, *Langmuir* **2006**, *22*, 5533.
[19] A. M. Cao, J. S. Hu, H. P. Liang, L. J. Wan, *Angew. Chem.* **2005**, *117*, 4465; *Angew. Chem. Int. Ed.* **2005**, *44*, 4391; *Angew. Chem.* **2005**, *117*, 4465.
[20] N. Bahlawane, P. A. Premkumar, K. Onwuka, G. Reiss, K. Kohse-Höinghaus, *Microelectron. Eng.* **2007**, *84*, 2481.
[21] N. Bahlawane, P. A. Premkumar, K. Onwuka, K. Rott, G. Reiss, K. Kohse-Höinghaus, *Surf. Coat. Technol.* **2007**, *201*, 8914.
[22] M. Imada, A. Fujimori, Y. Tokura, *Rev. Mod. Phys.* **1998**, *70*, 1039.
[23] K. L. Holman, T. M. McQueen, A. J. Williams, T. Klimczuk, P. W. Stephens, H. W. Zandbergen, Q. Xu, F. Ronning, R. J. Cava, *Phys. Rev. B* **2009**, *79*, 245114.
[24] C. N. Berglund, H. J. Guggenheim, *Phys. Rev.* **1969**, *185*, 1022.

